ACS APPLIED MATERIALS & INTERFACES

Research Article

www.acsami.org

Nano–Micrometer-Architectural Acidic Silica Prepared from Iron Oxide of *Leptothrix ochracea* Origin

Hideki Hashimoto,[†] Atsushi Itadani,[†] Takayuki Kudoh,[†] Satoshi Fukui,[‡] Yasushige Kuroda,[†] Masaharu Seno,[†] Yoshihiro Kusano,[§] Yasunori Ikeda,[∥] Yasuhiko Benino,[‡] Tokuro Nanba,[‡] Makoto Nakanishi,[†] Tatsuo Fujii,[†] and Jun Takada[†,⊥,*]

[†]Graduate School of Natural Science and Technology and [‡]Graduate School of Environmental Science, Okayama University, Okayama 700-8530, Japan

[§]Department of Fine and Applied Arts, Kurashiki University of Science and the Arts, Kurashiki, Okayama 712-8505, Japan

[∥]Research Institute for Production Development, Sakyo-ku, Kyoto 606-0805, Japan

[⊥]JST, CREST, Okayama 700-8530, Japan

Supporting Information

ABSTRACT: We prepared nano–micrometer-architectural acidic silica from a natural amorphous iron oxide with structural silicon which is a product of the iron-oxidizing bacterium *Leptothrix ochracea*. The starting material was heat-treated at 500 °C in a H_2 gas flow leading to segregation of α-Fe crystalline particles and then dissolved in 1 M hydrochloric acid to remove the α-Fe particles, giving a gray-colored precipitate. It was determined to be amorphous silica containing some amount of iron (Si/Fe = ∼60). The amorphous silica maintains the nano–microstructure of the starting material—∼1-μm-diameter micrometer-tubules consisting of inner globular and outer fibrillar structures several tens of nanometer in size—and has many large pores which are most probably formed as a result of segregation of the α-Fe particles on the micrometer-tubule wall. The smallest particle size of the amorphous silica is ∼10 nm, and it has a large surface area of 550 m^2/g with micropores (0.7 nm). By using pyridine vapor as a probe molecule to evaluate the active sites in the amorphous silica, we found that it has relatively strong Brønsted and Lewis acidic centers that do not desorb pyridine, even upon evacuation at 400 °C. The acidity of this new silica material was confirmed through representative two catalytic reactions: ring-opening reaction and Friedel–Crafts-type reaction, both of which are known to require acid catalysts.

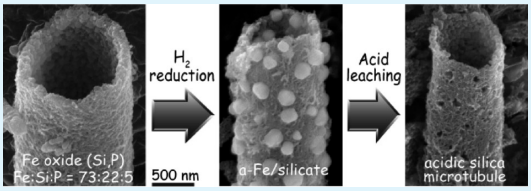

KEYWORDS: *amorphous silica, Brønsted acid, Lewis acid, acid catalysts, iron-oxidizing bacteria, biogenous iron oxides*

INTRODUCTION

Industrially synthesized amorphous silica is used in many applications, most commonly as adsorbents and also as additives in foods and medicines. Other representative silicon-containing oxide materials—such as synthesized and natural zeolites (SiO_2/Al_2O_3) with very strong Brønsted and Lewis acid sites—are used as solid acid catalysts for chemical reactions such as cracking, isomerization, and alkylation.[1]

Numerous studies have been reported recently on porous amorphous silica materials. Their morphologies, pores, and surface properties can be controlled precisely by artificial processes.[2−13] For instance, silica nanotubes and mesoporous silica have been developed, and their applications to biological, environmental, and biomedical fields and as solid catalysts have been proposed.[2−13] Silica nanotubes with various morphologies including single, double, helical, and ribbon structures are expected to be used in a wide range of applications such as chemosensors and heavy-metal-ion adsorbents[2,3] as well as drug-delivery systems and single-DNA sensors.[4−6] Mesoporous silica (e.g., FSM-16 and MCM-41) is expected to be used as a selective catalyst for chemical reactions since it has an active acid center.[7−13] In recent years, another notable study on mesoporous silica using the biomimetic approach was reported and attracted many researchers' attention.[14] Clearly, the development of novel porous silica materials with unique nanostructures and/or acid sites is promising and potentially important in various fields of science and industry. Our objective in this study is to prepare novel nano–micrometer-architectural acidic amorphous silica from Si-containing natural iron oxides produced by iron-oxidizing bacteria which we call "biogenous iron oxides (BIOXs)".

Iron-oxidizing bacteria live in aquatic environments of ambient temperature and pressure and neutral pH, where they derive energy by oxidizing Fe^{2+} in groundwater to Fe^{3+}.[15,16] As a result of this oxidation process, extracellular iron oxide precipitates with unique morphologies such as ∼1-μm-diameter micrometer-tubules and twisted stalks form near their cells.[15,16] Although these bacteria and BIOXs have been studied from mostly microbiological and geochemical perspectives,[15,16] we have been investigating their potential applications

Received: March 21, 2013
Accepted: May 14, 2013
Published: May 14, 2013

   dx.doi.org/10.1021/am401029r | ACS Appl. Mater. Interfaces 2013, 5, 5194−5200

for various industrial fields such as catalysts, catalyst supports, pigments, and magnetic materials.[17−23] The target BIOX in this study is iron oxide micrometer-tubules (*L*-BIOX) produced by *Leptothrix ochracea*.[24] *L*-BIOX is primarily composed of amorphous iron oxide (Fe:Si:P = 73:22:5 in an atomic ratio, with the exception of oxygen, hydrogen, and carbon) nanoparticles ∼3 nm across.[25] The primary nanoparticles are aggregated into secondary globular and fibrillar structures on the order of several tens of nanometers, and finally these particles are intricately interconnected into micrometer tubules that are ∼1 μm in diameter.[18,26] The silicon in *L*-BIOX seems to be an attractive silica source and the porous nano−microstructure of *L*-BIOX also seems to be an attractive character. We recently reported that acidic amorphous silica prepared from *L*-BIOX works as a solid acid catalyst for chemical reactions.[23] However, the unique morphological structure of *L*-BIOX was not retained in our previously reported silica.

Herein, we describe the two-step preparation of novel nano−micrometer-architectural acidic silica from natural *L*-BIOX as a starting material. Its preparation method and basic characteristics including nano−microstructural, compositional, and porous features and acidic properties are reported.

EXPERIMENTAL SECTION

Sample Preparation and Characterization. *L*-BIOX was obtained as an ocher precipitate from a groundwater purifying tank.[17] It was washed repeatedly with distilled water,[17] dried in air at 100 °C, heat-treated at various temperatures (300, 400, 450, 500, 550, 600, and 700 °C) in a H_2 (purity 4 nines) gas flow for 1 h at a heating rate of 10 °C/min, and allowed to cool in the furnace. The heat-treated sample was added to 1 M hydrochloric acid solution at room temperature (RT) and stirred for 1 h. The resulting precipitate was filtered, washed with distilled water, and vacuum-dried.

The samples were evaluated by the following analytical methods. Crystallographic and morphological features were examined by X-ray diffractometry (XRD; RINT-2000, Rigaku, Japan), scanning electron microscopy (SEM; S-4300, Hitachi, Japan), and transmission electron microscopy (TEM; JEM-2100F, JEOL, Japan). Elemental analysis was performed by energy dispersive X-ray spectroscopy (EDX; Genesis 2000 for SEM, Ametek, Japan) and inductively coupled plasma mass spectroscopy (ICP-MS; ELAN DRC-II, PerkinElmer, Japan). Surface area and pore size distribution were calculated by Brunauer−Emmett−Teller (BET) method,[27] micropore analysis (MP) method,[28] and Dollimore−Heal (DH) method[29,30] from nitrogen adsorption isotherms measured at −196 °C (BELSORP-mini-II; BEL Japan). To investigate thermostability of the acid-leaching sample of 500 °C-heat-treated sample, it was heat-treated at 900, 1000, 1100, 1200, and 1300 °C in air, and its microstructure was evaluated by SEM.

Evaluation of Acidic Centers. Surface state of the acid-leaching sample of 500 °C-heat-treated sample was characterized by the following analytical methods. Diffuse reflectance ultraviolet visible near-infrared (DR UV−Vis−NIR) spectra of the sample and *L*-BIOX were measured at RT using a JASCO V-570 UV/vis/NIR spectrophotometer (JASCO Co., Japan) equipped with an integral sphere. Sample pretreatment was carried out by evacuation at RT for 2 h under a reduced pressure of 1.3 mPa. Electron paramagnetic resonance (EPR) spectrum of the sample was recorded at RT by a JEOL-FE3XG spectrometer operating at ∼9.5 GHz (field modulation, 100 kHz; microwave power, 1 mW; and modulation width, 5 G). The sample (∼25 mg) was loaded into the EPR sample tube. The resonance magnetic field was determined by using a manganese species doped into the solid material as a reference. Because infrared (IR) spectroscopy of adsorbed probe molecules is commonly employed, a useful technique for clarifying the state of solid surface,[31,32] the solid acid properties were investigated by Fourier transform infrared (FTIR) spectroscopy. FTIR spectra were measured at RT by FTIR spectrophotometer (FTS4000MXK, Digilab, Randolph NJ, USA) with a mercury−cadmium−telluride (MCT) detector kept at liquid-N_2 temperature. A total of 144 detector readings were accumulated at a spectral resolution of 2 cm^{-1}. The sample (∼8 mg) was pressed into a 10-mm pellet and placed in a quartz cell with KRS-5 windows that enables sample pretreatment and gas introduction in situ.[33] Sample pretreatment was performed by evacuation at RT for 2 h under a reduced pressure of 1.3 mPa. The sample was then exposed to pyridine vapor (Py; purity 99.8%; Sigma-Aldrich) at a pressure of ∼26 Pa at RT. After adsorption, the sample was again treated at various temperatures (200, 400, 600 °C) for 1 h under a reduced pressure of 1.3 mPa.

General Procedure of Catalytic Reactions. The catalytic activity of the silica sample, *L*-BIOX, and previously reported biogenous silica (BSL) sample was evaluated for the ring-opening reaction of styrene oxide (Scheme 1a) and the Friedel−Crafts reaction of indole with methyl vinyl ketone (Scheme 1b). These reactions were conducted under ordinary conditions, and the reaction products were characterized by ^{1}H NMR (600 VNMRS, Varian) and analytical thin-layer chromatography (TLC).

Scheme 1. (a) Ring-Opening Reaction of an Epoxide and (b) Friedel−Crafts-Type Alkylation

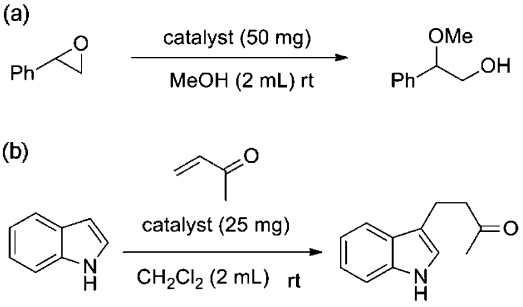

Ring-Opening Reaction of Styrene Oxide. First, to a solution of styrene oxide (0.12 mL, 1 mmol) in methanol (2 mL) was added the catalyst (50 mg) at RT, and the suspension was stirred until the reaction was complete as determined by TLC. The methanol was then removed using a rotary evaporator. The resultant residue was purified by column chromatography on silica gel (88:12−75:25 hexane/ethyl acetate) to give a colorless oil. ^{1}H NMR (600 MHz, NMR) δ 3.14 (s, 3H), 3.53 (dd, 1H, J = 3.7, 11.7 Hz), 3.59 (dd, 1H, J = 8.6, 11.7 Hz), 4.22 (dd, 1H, J = 3.7, 8.6 Hz), 7.2−7.4 (m, 5H).

Friedel−Crafts Reaction of Indole with Methyl Vinyl Ketone. First, to a solution of indole (50 mg, 0.427 mmol) in CH_2Cl_2 (2 mL) was added methyl vinyl ketone (0.1 mL, 1.23 mmol). Second, a catalyst (25 mg) was added to this solution at RT. Third, the suspension was stirred until the reaction was complete as determined by TLC. Next, the suspension was purified by column chromatography on silica gel (88:12−75:25 hexane/ethyl acetate) to give a white solid. ^{1}H NMR (600 MHz, $CDCl_3$) δ 2.07 (s, 3H), 2.78 (t, 2H, J = 7.6 Hz), 2.85 (t, 2H, J = 7.6 Hz), 6.92 (s, 1H), 7.0−7.6 (m, 4H), 7.88 (b, 1H).

RESULTS AND DISCUSSION

Figure 1 shows XRD patterns of *L*-BIOX and the samples heat-treated in a H_2 gas flow. *L*-BIOX shows two broad diffraction peaks corresponding to *d*-spacing values of 0.27 and 0.15 nm, indicating its amorphousness (Figure 1a).[17,25] With heat treatment, the peaks change as follows. At 300 °C, both peaks sharpen slightly (Figure 1b). At 400 °C, metallic iron (α-Fe) begins to form (Figure 1c). At >400 °C, the peaks of α-Fe continue to sharpen (Figure 1d−h), and the very broad diffraction peak near a *d*-spacing value of 0.27 nm, indicating the presence of poorly crystalline iron oxides, continues to broaden. At 550 °C, the latter peak essentially vanishes (Figure

dx.doi.org/10.1021/am401029r | ACS Appl. Mater. Interfaces 2013, 5, 5194−5200

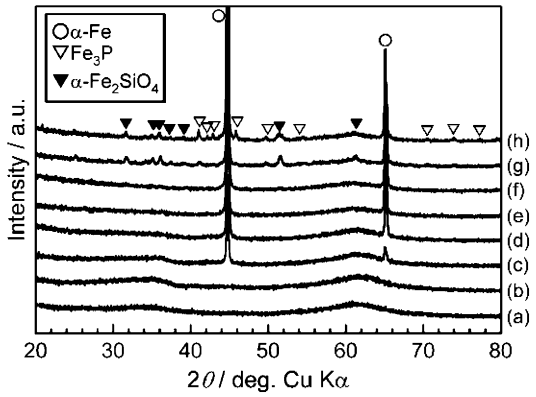

Figure 1. XRD patterns of (a) untreated *L*-BIOX and of *L*-BIOX heat-treated at (b) 300, (c) 400, (d) 450, (e) 500, (f) 550, (g) 600, and (h) 700 °C in a H_2 gas flow.

1f), suggesting that most of the Fe^{3+} in *L*-BIOX has reduced to the metallic state. At ≥600 °C, α-Fe_2SiO_4 and Fe_3P form (Figure 1g,h).

Figure 2 shows SEM images of the samples heat-treated in a H_2 gas flow that confirm these morphological changes. *L*-BIOX

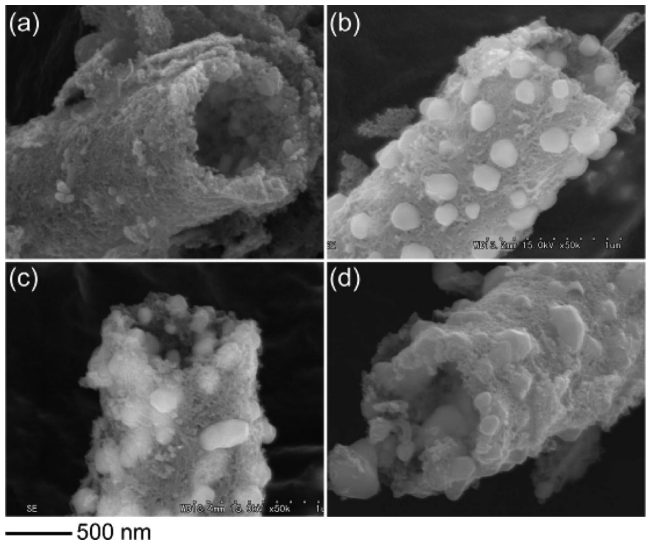

Figure 2. SEM images of *L*-BIOX heat-treated at (a) 400, (b) 500, (c) 600, and (d) 700 °C in a H_2 gas flow.

before heat treatment is known to have a ∼1-μm-diameter microtubular form that consists of inner globular and outer fibrillar structures on the order of several tens of nanometers.[26] The samples heat-treated at 400 °C (Figure 2a) and ≥500 °C (Figure 2b–d) have relatively small (avg. 80 nm) and remarkably large (avg. 180 nm) particles, respectively, on the inner and outer surfaces of the micrometer-tubule walls, which we presume to be α-Fe crystals. The samples heat-treated at 500 °C (Figure 2b) and 600 °C (Figure 2c) have tubule outer diameters that have shrunk slightly from 1.35 μm (for *L*-BIOX before heat treatment) to 1.21 and 0.99 μm, respectively (estimated shrinking ratios = 10% and 27%). The samples heat-treated at all temperatures have maintained the nanostructure and microstructure of the starting material: outer fibrillar and inner globular structures constituting an overall microtubular structure.

Our previous studies showed that *L*-BIOX contains structural Si and P in the ratio Fe:Si:P = 73:22:5 (atom %) with the exception of O, H, and C. The elements are distributed evenly, and Si–O–Fe chemical linkages exist.[20] These background and the aforementioned XRD and SEM results lead us to suggest that, during heating in a H_2 gas flow, the Si–O–Fe linkages cleave, Fe concentrates to form α-Fe, and Si concentrates to form Si–O–Si linkages (silicate matrix). α-Fe crystalline particles and silicate micrometer-tubule matrixes then form as shown in Figure 2. At relatively high temperature of 600 and 700 °C, Si and P in the silicate matrix react with α-Fe and/or residual Fe component in silicate matrix to form α-Fe_2SiO_4 and Fe_3P.

With these results in hand, we formulated the goal of separating silica micrometer tubules from crystalline α-Fe, α-Fe_2SiO_4, and Fe_3P in acidic solution. Accordingly, we subjected the heat-treated samples to acid-leaching in 1 M hydrochloric acid solution. Figure 3 shows representative XRD patterns of

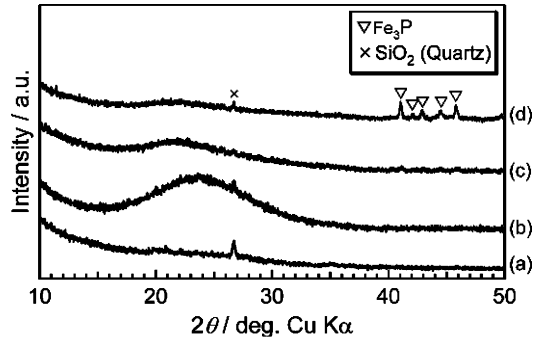

Figure 3. XRD patterns of acid-leached *L*-BIOX samples that had previously been heat-treated at (a) 450, (b) 500, (c) 600, and (d) 700 °C in a H_2 gas flow. The small SiO_2 (quartz) peak observed for all samples results from contamination from groundwater that is used as a source of *L*-BIOX.

the acid-leaching heat-treated samples. All samples show a broad diffraction peak near d = 0.39 nm, indicating the presence of amorphous silica. The diffraction patterns differ as follows: that for the sample heat-treated at 450 °C shows an extremely weak diffraction peak (Figure 3a); that for the sample heat-treated at 500 °C shows most pronounced peak (Figure 3b); those for the samples heat-treated at 600 and 700 °C show the presence of Fe_3P crystals (Figure 3c,d).

Figure 4 shows SEM images of the acid-leaching heat-treated samples. All samples except for that heat-treated at 400 °C maintain a tubular form with the inner globular and outer fibrillar structures of *L*-BIOX (Figure 4b–d). The samples heat-treated at 600 and 700 °C still contain crystalline particles considered to be Fe_3P (Figure 4e,f). The sample heat-treated at 500 °C with the most pronounced XRD peak (d = 0.39 nm) (Figure 3b) contains no crystalline particles but does contain many large pores, indicating segregation of α-Fe at the inner and outer surfaces of the micrometer tubules (Figure 4c,d). Surprisingly, even though the silica component in the starting material constitutes no more than 13.5 wt %, the sample heat-treated at 500 °C has maintained the nanostructure (outer fibrillar and inner globular structures) and microstructure (microtubular structure) of the starting material (Figure 4c,d).

EDX analysis shows compositional features of the acid-leaching samples. The sample heat-treated at 450 °C is composed almost solely of Si and O with some amount of

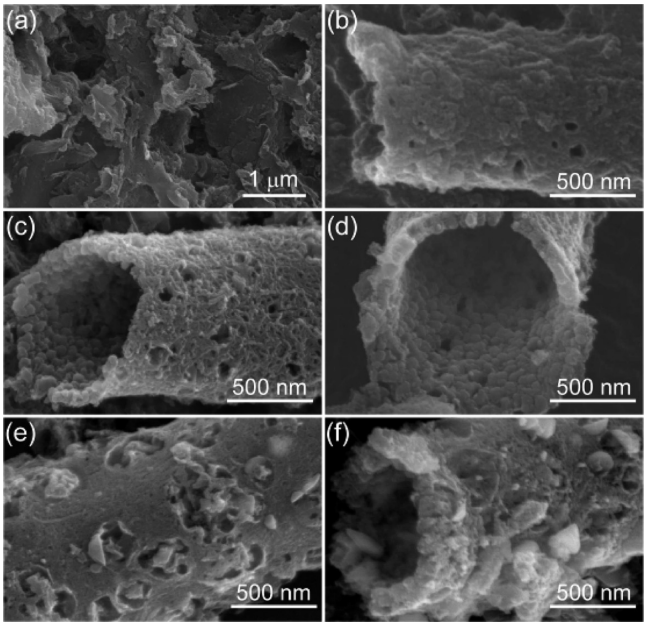

Figure 4. SEM images of acid-leached *L*-BIOX samples that had previously been heat-treated at (a) 400, (b) 450, (c and d) 500, (e) 600, and (f) 700 °C in a H_2 gas flow.

Fe; the sample heat-treated at 500 °C is composed of only Si and O; and the samples heat-treated at 600 and 700 °C are composed almost solely of Si and O with some amounts of Fe and P attributed to Fe_3P. The sample heat-treated at 500 °C is of particular interest, and we conclude that we have successfully prepared silica micrometer tubules by acid leaching of the sample heat-treated at 500 °C in a H_2 gas flow. We call this sample biogenous silica micrometer tubule (BSL-MT) hereafter. The remainder of this study is devoted to a detailed investigation of its features.

The Si/Fe ratio of BSL-MT, measured by ICP-MS, is ∼60, showing that the sample contains some amounts of Fe. Figure 5 shows TEM images of BSL-MT. The outer diameter of micrometer tubule has shrunk from 1.35 μm (for *L*-BIOX before heat treatment) to 1.21 μm for the sample heat-treated at 500 °C and 0.93 μm for BSL-MT (estimated shrinking ratios = 10 and 31%) (Figure 5a). The ED pattern for a single BSL-MT shows a halo pattern, indicating structural amorphousness (Figure 5b, inset), well-consistent with the XRD result (Figure 3b). Many large pores are present on the micrometer-tubule wall (Figure 5b,c), as might form when α-Fe particles dissolve in acid solution. Although the inner globular and outer fibrillar structures are preserved, fine primary particles ∼3 nm in diameter observed in *L*-BIOX[18,26] are not observed (Figure 5 d,e). We presume that primary particles of *L*-BIOX might grow to form a silicate matrix when *L*-BIOX is heat-treated in a H_2 gas flow. The smallest particle size we observed here is ∼10 nm (Figure 5e), but particle shapes and sizes are various and inhomogeneous. The BET surface area of BSL-MT, calculated from nitrogen adsorption isotherms, is a very large value of 550 m^2/g, which is twice larger than that of original *L*-BIOX (280 m^2/g).[18] Pore size distribution, as calculated by the MP and DH methods, reveals that BSL-MT is porous, with micropores of d_p = 0.7 and a very small amount of mesopores of r_p <40 nm (Figure 6). Some of such micropores and mesopores could

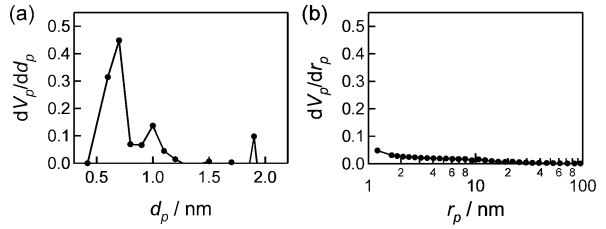

Figure 6. (a) Micropore and (b) mesopore size distributions of acid-leached *L*-BIOX samples that had previously been heat treated at 500 °C in a H_2 gas flow, calculated by the MP and DH methods, respectively.

form at interspaces of aggregated primary particles and/or inside of the primary particles. The chemical formula with structural OH groups excluding physisorbed water is $SiO_2 \cdot 0.4H_2O$, based on weight change under heating at 1000 °C for 2 h as measured by thermogravimetry. We considered the weight losses below and above 130 °C to be attributed to dehydration of physisorbed water and structural OH groups, respectively. Additionally, we investigated thermostability of nano−microstructure of BSL-MT (see Supporting Information Figure S1). The micrometer-tubule structure was maintained up to 1100 °C but was shrunk a little. Above 1200 °C, the bore of the tubules was closed by sintering of the particles and tubules changed to rods. Outer fibrillar and inner globular structures of the tubules and pores of the tubule wall were maintained up to 1000 °C and were sintered above 1100 °C. These results suggest that nano−microstructure of BSL-MT has relatively high thermostability.

We examined the surface state of BSL-MT from the DR UV−vis−NIR, EPR, and IR spectroscopies. Figure 7a shows the DR UV−vis−NIR spectrum for *L*-BIOX and BSL-MT

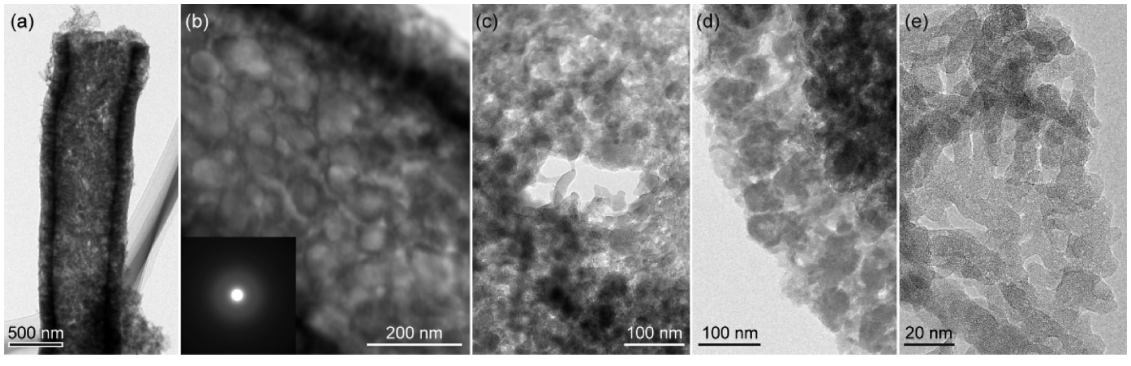

Figure 5. TEM images of acid-leached *L*-BIOX samples that had been heat-treated at 500 °C in a H_2 gas flow.

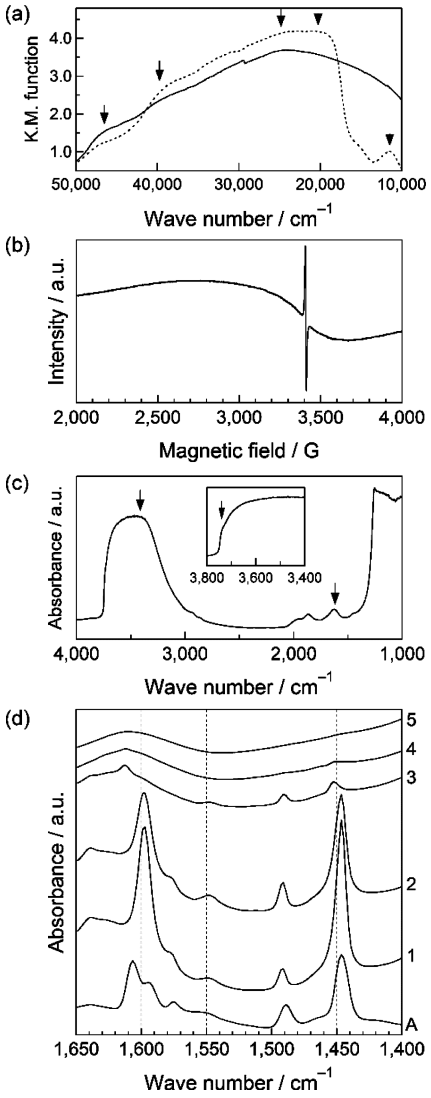

Figure 7. (a) DR UV−vis−NIR spectrum of BSL-MT (solid line) and *L*-BIOX (dotted line) treated at RT. (b) EPR spectrum of BSL-MT recorded at RT. (c) IR spectrum of BSL-MT evacuated at RT. (d) IR spectra of BSL-MT after various treatments: (1) after exposure to Py vapor at ∼26 Pa at RT; (2−5) after re-evacuation at RT, 200, 400, and 600 °C, respectively. (A) Spectra of *L*-BIOX exposed to Py under the same conditions as for BSL-MT.

treated at RT. For *L*-BIOX, the typical bands which are due to Fe_2O_3 species are observed at around 20 000 and 13 000 cm^{-1} (arrowheads in Figure 7a), whereas for BSL-MT such bands are scarcely observed, and the bands at around 46 000, 40 000, and 25 000 cm^{-1} (arrows in Figure 7a) are clearly observed, indicating that acid-leaching of the heat-treated sample apparently removes iron oxide species. However, the quantitative discussion is difficult from the present data. The former bands at 46 000 and 40 000 cm^{-1} are ascribed to the transitions with ligand to metal (i.e., Fe^{3+}) charge transfer character, and the band at 25 000 cm^{-1} is due to the d−d transitions of Fe^{3+} in tetrahedral symmetry.[34,35] Figure 7b shows the EPR spectrum recorded at RT for BSL-MT. A broad band observed in the whole range of measurement is due to some amount of Fe^{3+} species in BSL-MT.[36] A sharp band clearly appears at around 3400 G (g = 2.003), which is close to the value of the free electron (g = 2.0023). Referring to the report made by Inaki et al.,[37] the defect sites such as ≡Si−O• and Si• which were formed through the cleavage of strained siloxane bridge (Si−O−Si linkage forming the pore) could be formed in BSL-MT. In the IR spectrum for the BSL-MT sample treated at RT, the broad bands are observed at 3300 and 1630 cm^{-1} (arrows in Figure 7c). These bands are assigned to O−H stretching and bending vibrations in physisorbed water molecules into the pores, respectively.[38,39] In addition, the band at around 3741 cm^{-1} also appears (arrow in inset to Figure 7c), which is due to the O−H stretching mode of OH groups attached to Si (i.e., Si−OH).[40−43]

As described in our previous report,[23] we investigated the solid acid property of the direct acid-leaching sample of *L*-BIOX that we call biogenous silica (BSL) by IR spectroscopy using Py as a probe molecule. Interestingly, although pure silica is known to be neutral or very slightly acidic, BSL has relatively strong Brønsted and Lewis acid sites, perhaps because small amount of Fe^{3+} is present in the BSL structure (Si/Fe = ∼150) and/or BSL has lattice structural distortion.[23] Because BSL-MT also contains some amount of Fe (Si/Fe = ∼60), it may have analogous acid sites as BSL. Figure 7d shows IR spectra for *L*-BIOX treated at RT and BSL-MT treated under various conditions. As with *L*-BIOX, BSL-MT that has been exposed to Py at RT shows characteristic IR bands assignable to hydrogen-bonded Py species (∼1600, ∼1450, and ∼1490 cm^{-1}),[44] Py species adsorbed on both Lewis and Brønsted acid sites (∼1480 cm^{-1}), and Py species adsorbed on Lewis acid (∼1600 and ∼1450 cm^{-1}) or Brønsted acid (1640 and 1548 cm^{-1}) sites.[45−47] Py species adsorbed onto BSL-MT desorbed completely with re-evacuation at around 400 °C. Thus, we have confirmed the existence in BSL-MT of relatively strong Lewis and Brønsted acid sites. According to the aforementioned EPR and IR spectra (Figure 7b,c), BSL-MT has the strained siloxane bridge (Si−O−Si) and silanol group (Si−OH), suggesting the formation of Si−OH^+−Si and SiO^- species near the cleavage of Si−O−Si linkage; the former Si−OH^+−Si species could work as the acidic site in BSL-MT. Therefore, we conclude that the origin of acidic centers of this material could be due to both some amount of Fe^{3+} and lattice structural distortion.

We checked whether the acid sites characterized by the above IR spectroscopy work as active sites for organic reactions. Two typical acid-catalyzed organic reactions, a ring opening of an epoxide and a Friedel−Crafts-type alkylation (Scheme 1), were examined. In these reactions, acid sites of catalysts activate the epoxide (Scheme 1a) and the carbonyl functional group of methyl vinyl ketone (Scheme 1b). *L*-BIOX and our previously developed silica material BSL, which has relatively strong active sites,[23] were also used as reference catalysts for these reactions. All reactions were monitored by TLC analysis at appropriate time intervals, and all reactions were stopped at the time to reach reaction equilibrium of BSL-MT: 21 h and 3 days for reactions (a) and (b), respectively. Table 1 shows the reaction results. In both reactions, BSL-MT effectively catalyzed the reactions to give products in good yields (67% and 93% for

Table 1. Reaction Yields for Different Silica Catalysts

	reaction (a)		reaction (b)	
catalyst	yield, %	time	yield, %	time
BSL-MT	67	21 h	93	3 days
BSL	41	21 h	40	3 days
L-BIOX	29	21 h	7	3 days

dx.doi.org/10.1021/am401029r | ACS Appl. Mater. Interfaces 2013, 5, 5194−5200

reactions (a) and (b), respectively), while BSL gave moderate (41% and 40% for reactions (a) and (b), respectively) and *L*-BIOX gave poor (29% and 7% for reactions (a) and (b), respectively) yields. These results indicate that the BSL-MT surface certainly has active acidic sites for organic reactions. Interestingly, BSL-MT exhibits higher acid catalytic activity than do our previously developed BSL,[23] even though both are prepared from the same *L*-BIOX. This result suggests that the microtubular shape and/or iron content of BSL-MT could be related to its catalytic activity. Experimental studies to elucidate the relation among structure, composition, and catalytic activity for these silica samples are currently underway in our group.

We also performed the same H_2-reducing and acid-leaching experiment with BIOXs produced by *L. ochracea* and *Gallionella ferruginea* from another sampling site at Okayama University.[26,48] Regardless of sampling site, bacterial species, morphologies, and chemical composition, we obtained amorphous silica with unique morphologies (micrometer-tubules from *L. ochracea* and twisted stalks from *G. ferruginea*) and nearly the same acid properties as for BSL-MT in this study. These results indicate that any Si-containing BIOXs with unique morphologies can be transformed into acidic amorphous silica with the same unique morphology. We expect to develop further applications of our new silica materials beyond that of solid acid catalyst in the near future.

CONCLUSIONS

We synthesized novel amorphous silica micrometer-tubules from a unique starting material: iron oxide micrometer-tubules composed of Si-containing amorphous iron oxide nanoparticles produced by iron-oxidizing bacteria. The iron oxide was heat-treated at 500 °C in a H_2 gas flow and then dissolved in concentrated hydrochloric acid and dried, giving amorphous silica. Remarkably, the formed silica almost retains the nano−micrometer-architectural structure of its starting material: outer fibrillar and inner globular structures several tens of nanometers in size that comprise micrometer tubules ∼1 μm in diameter. This new biogenous silica micrometer-tubule material, with relatively strong acidic centers and high surface area with distinctive micropores, serves as an effective acid catalyst for ring-opening and Friedel−Crafts reactions.

ASSOCIATED CONTENT

Supporting Information

SEM images. This material is available free of charge via the Internet at http://pubs.acs.org.

AUTHOR INFORMATION

Corresponding Author

*E-mail: jtakada@cc.okayama-u.ac.jp.

Notes

The authors declare no competing financial interest.

ACKNOWLEDGMENTS

The authors thank Mr. K. Yamashita, Mr. Y. Yamano, Mr. Y. Kishimoto, and Mr. M. Nakamura for helpful discussions. This study was financially supported by a Special Grant for Education and Research from the Ministry of Education, Culture, Sports, Science, and Technology, Japan, and JSPS KAKENHI Grants 2465408904, 24510151, 24760550, and 23360309.

REFERENCES

(1) Wang, W.; Hunger, M. *Acc. Chem. Res.* **2008**, *41*, 895−904.
(2) Bommel, K. J. C.; Friggeri, A.; Shinkai, S. *Angew. Chem., Int. Ed.* **2003**, *42*, 980−999.
(3) Jung, J. H.; Park, M.; Shinkai, S. *Chem. Soc. Rev.* **2010**, *39*, 4286−4302.
(4) Son, S. J.; Reichel, J.; He, B.; Schuchman, M.; Lee, S. B. *J. Am. Chem. Soc.* **2005**, *127*, 7316−7317.
(5) Fan, R.; Karnik, R.; Yue, M.; Li, D.; Majumdar, A.; Yang, P. *Nano Lett.* **2005**, *5*, 1633−1637.
(6) Lee, S. B.; Mitchell, D. T.; Trofin, L.; Nevanen, T. K.; Soderlund, H.; Martin, C. R. *Science* **2002**, *296*, 2198−2200.
(7) Kresge, C. T.; Leonowicz, M. E.; Roth, W. J.; Vartuli, J. C.; Beck, J. S. *Nature* **1992**, *359*, 710−712.
(8) Corma, A. *Chem. Rev.* **1997**, *97*, 2373−2419.
(9) Thomas, J. M. *Angew. Chem., Int. Ed.* **1999**, *38*, 3588−3628.
(10) Ishitani, H.; Iwamoto, M. *Tetrahedron Lett.* **2003**, *44*, 299−301.
(11) Iwamoto, M.; Tanaka, Y.; Sawamura, N.; Namba, S. *J. Am. Chem. Soc.* **2003**, *125*, 13032−13033.
(12) Haishi, T.; Kasai, K.; Iwamoto, M. *Chem. Lett.* **2011**, *40*, 614−616.
(13) Yamamoto, T.; Tanaka, T.; Funabiki, T.; Yoshida, S. *J. Phys. Chem. B* **1998**, *102*, 5830−5839.
(14) Jensen, M.; Keding, R.; Höche, T.; Yue, Y. *J. Am. Chem. Soc.* **2009**, *131*, 2717−2721.
(15) Ghiorse, W. C. *Annu. Rev. Microbiol.* **1984**, *38*, 515−550.
(16) Emerson, D.; Fleming, E. J.; McBeth, J. M. *Annu. Rev. Microbiol.* **2010**, *64*, 561−583.
(17) Hashimoto, H.; Yokoyama, S.; Asaoka, H.; Kusano, Y.; Ikeda, Y.; Seno, M.; Takada, J.; Fujii, T.; Nakanishi, M.; Murakami, R. *J. Magn. Magn. Mater.* **2007**, *310*, 2405−2407.
(18) Ema, T.; Miyazaki, Y.; Kozuki, I.; Sakai, T.; Hashimoto, H.; Takada, J. *Green Chem.* **2011**, *13*, 3187−3195.
(19) Mandai, K.; Korenaga, T.; Ema, T.; Sakai, T.; Furutani, M.; Hashimoto, H.; Takada, J. *Tetrahedron Lett.* **2012**, *53*, 329−332.
(20) Hashimoto, H.; Asaoka, H.; Nakano, T.; Kusano, Y.; Ishihara, H.; Ikeda, Y.; Nakanishi, M.; Fujii, T.; Yokoyama, T.; Horiishi, N.; Nanba, T.; Takada, J. *Dyes Pigm.* **2012**, *95*, 639−643.
(21) Hashimoto, H.; Fujii, T.; Nakanishi, M.; Kusano, Y.; Ikeda, Y.; Takada, J. *Mater. Chem. Phys.* **2012**, *136*, 1156−1161.
(22) Hashimoto, H.; Itadani, A.; Fujii, T.; Nakanishi, M.; Asaoka, H.; Kusano, Y.; Ikeda, Y.; Kuroda, Y.; Takada, J. *Mater. Res. Bull.* **2013**, *48*, 1174−1177.
(23) Hashimoto, H.; Itadani, A.; Kudoh, T.; Kuroda, Y.; Seno, M.; Kusano, Y.; Ikeda, Y.; Nakanishi, M.; Fujii, T.; Takada, J. *ACS Appl. Mater. Interfaces* **2013**, *5*, 518−523.
(24) Spring, S. In *The Prokaryotes*; Dworkin, M., Falkow, S., Rosenberg, E., Schleifer, K. H., Stackebrandt, E., Eds.; Springer: New York, 2006; Vol. *5*, p 758.
(25) Hashimoto, H.; Fujii, T.; Kohara, S.; Asaoka, H.; Kusano, Y.; Ikeda, Y.; Nakanishi, M.; Benino, Y.; Nanba, T.; Takada, J. *Mater. Chem. Phys.* **2012**, *137*, 571−575.
(26) Suzuki, T.; Hashimoto, H.; Ishihara, H.; Kasai, T.; Kunoh, H.; Takada, J. *Appl. Environ. Microbiol.* **2011**, *77*, 7873−7875.
(27) Brunauer, S.; Emmett, P. H.; Teller, E. *J. Am. Chem. Soc.* **1938**, *60*, 309−319.
(28) Mikhail, R. S.; Brunauer, S.; Bodor, E. *J. Colloid Interface Sci.* **1968**, *26*, 45−53.
(29) Dollimore, D.; Heal, G. *J. Appl. Chem.* **1964**, *14*, 109−114.
(30) Dollimore, D.; Heal, G. *J. Colloid Interface Sci.* **1970**, *33*, 508−519.
(31) Davydov, A. A. In *Infrared spectroscopy of adsorbed species on the surface of transition metal oxides*; John Wiley & Sons Inc.: New York, 1984.
(32) Lamberti, C.; Zecchina, A.; Groppo, E.; Bordiga, S. *Chem. Soc. Rev.* **2010**, *39*, 4951−5001.
(33) Kuroda, Y.; Maeda, H.; Morimoto, T. *Rev. Sci. Instrum.* **1989**, *60*, 3083−3085.

(34) Inui, T.; Nagata, H.; Takeguchi, T.; Iwamoto, S.; Matsuda, H.; Inoue, M. *J. Catal.* **1993**, *139*, 482−489.
(35) Bordiga, S.; Buzzoni, R.; Geobaldo, F.; Lamberti, C.; Giamello, E.; Zecchina, A.; Leofanti, G.; Petrini, G.; Tozzola, G.; Vlaic, G. *J. Catal.* **1996**, *158*, 486−501.
(36) El-Malki, El-M.; van Santen, R. A.; Sachtler, W. M. H. *J. Phys. Chem. B* **1999**, *103*, 4611−4622.
(37) Inaki, Y.; Yoshida, H.; Yoshida, T.; Hattori, T. *J. Phys. Chem. B* **2002**, *106*, 9098−9106.
(38) Nakamoto, K. In *Infrared and Raman spectra of inorganic and coordination compounds*, 5th ed.; John Wiley & Sons: New York, 1997.
(39) Jitianu, A.; Crisan, M.; Meghea, A.; Rau, I.; Zaharescu, M. *J. Mater. Chem.* **2002**, *12*, 1401−1407.
(40) Vansant, E. F.; Van Der Voort, P.; Vrancken, K. C. *Stud. Surf. Sci. Catal.* **1995**, *93*, 59.
(41) Zecchina, A.; Bordiga, S.; Spoto, G.; Marchese, L.; Petrini, G.; Leofanti, G.; Padovan, M. *J. Phys. Chem. A* **1992**, *96*, 4985−4990.
(42) Zecchina, A.; Bordiga, S.; Spoto, G.; Marchese, L. *J. Phys. Chem.* **1992**, *96*, 4991−4997.
(43) Seehra, M. S.; Roy, P.; Raman, A.; Manivannan, A. *Solid State Commun.* **2004**, *130*, 597−601.
(44) Zaki, M. I.; Hasan, M. A.; Al-Sagheer, F. A.; Pasupulety, L. *Langmuir* **2000**, *16*, 430−436.
(45) Parry, E. P. *J. Catal.* **1963**, *2*, 371−379.
(46) Parker, L. M.; Bibby, D. M.; Burns, G. R. *J. Chem. Soc., Faraday Trans.* **1991**, *87*, 3319−3323.
(47) Buzzoni, R.; Bordiga, S.; Ricchiardi, G.; Lamberti, C.; Zecchina, A. *Langmuir* **1996**, *12*, 930−940.
(48) Suzuki, T.; Hashimoto, H.; Matsumoto, N.; Furutani, M.; Kunoh, H.; Takada, J. *Appl. Environ. Microbiol.* **2011**, *77*, 2877−2881.